

# X-Ray microanalysis of stratified specimens

Jean-Louis Pouchou

*Office National d'Etudes et Recherches Aéronautiques (O.N.E.R.A.), Department of Materials, 29 avenue de la Division Leclerc, 92320 Chatillon (France)*

(Received 10th September 1992; revised manuscript received 15th March 1993)

## Abstract

This paper presents a description of the state of the art methodology and software for the application of x-ray microanalysis to thin surface layers and more generally to the characterization of stratified specimens. The sensitivity of the technique to near-surface segregation is demonstrated. Some emphasis is given on the  $\phi(\rho z)$  function (the distribution in depth of the primary generated x-ray intensity), which is the key to all advanced quantitative procedures presently available. The main characteristics of the recently developed software packages *Strata* and *Multifilm* are briefly described (physical basis, incorporation of fluorescence by lines and continuum, graphically assisted modes of operation, iterative mode of operation for the automatic determination of compositions and thicknesses). The capability of the technique is illustrated by three different applications: a bilayer on a substrate (case with no common element), a coated fibre (case with common elements and very light element analysis), a coated substrate analyzed in various geometrical conditions and by an "as soon as possible" procedure.

**Keywords:** Stratified specimens; Thin surface layers; X-Ray microanalysis

For 25 years, electron probe x-ray microanalysis (XRMA) has been conventionally applied to bulk specimens to obtain elementary chemical analyses of microvolumes of the order of  $1 \mu\text{m}^3$ . Contrary to other analytical techniques, XRMA has the advantage of providing quantitative results in an absolute way, i.e. it is actually not necessary to refer to standards similar to the specimen. For a given characteristic line, any standard (pure or compound) containing the element of interest permits to define an experimental relative intensity  $k$  (usually called  $k$ -ratio in the case of a pure standard), which can be converted into a mass concentration by use of a "correction" procedure. However, the conventional quantitative procedures used for 20 years (the most popular was the ZAF method) had a

limited field of applicability: low absorption situations (less than 30% of the x-rays emitted in the spectrometer direction should be absorbed by the specimen itself), and homogeneous microvolumes.

During the nineteneighties, several groups have made a real effort to promote new procedures in order to overcome the above limitations, extend quantitative analysis to very light elements (low energy, i.e., strongly absorbed lines), and characterize specimens with a depth-dependent composition. The key to those problems is the  $\phi(\rho z)$  function, defined by Castaing [1] in his pioneering work, and representing the distribution in depth of the primary ionizations generated per incident electron in the target. New models based on accurate  $\phi(\rho z)$  descriptions are now superseding the conventional procedures, namely the gaussian MSG model of Packwood and Brown [2] and Packwood et al. [3] and the PAP and XPP models of Pouchou and Pichoir [4–6]. Although they use different starting points

*Correspondence to:* J.-L. Pouchou, Office National d'Etudes et Recherches Aéronautiques (O.N.E.R.A.), Dept. of Materials, 29 av. de la Division Leclerc, 92320 Chatillon (France).

and mathematical expressions, these models aim to produce realistic distributions in depth of the primary generated x-ray intensity, in a wide range of electron and x-ray energies. The reliability of their  $\phi(\rho z)$  parameterization permits to evaluate accurately the strong absorption effects for soft x-rays, and to compute directly, in the case of stratified specimens, meaningful values of the x-ray intensity emitted by a surface layer, a buried layer, or a substrate.

This paper gives experimental evidences of the sensitivity of XRMA to the surface. Some basic principles are then recalled. Typical problems of near-surface analysis that can be solved in an effective manner by advanced x-ray microanalysis procedures are presented. The new computer programs *Strata* and *Multifilm*, developed recently in cooperation with SAMx on the basis of our PAP and XPP models, are used for this purpose.

#### ANALYZED DEPTH AND SENSITIVITY

As far as the resolution in depth is concerned, x-ray microanalysis under electron beam bombardment cannot compete with surface techniques like Auger emission spectrometry, x-ray photoelectron spectrometry or secondary ion mass spectrometry: in practice, as shown in Fig. 1, the depth of x-ray production cannot be significantly less than about  $10 \mu\text{g}/\text{cm}^2$  (i.e. 10 nm for a material with a density of  $10 \text{ g}/\text{cm}^3$ ), even in the

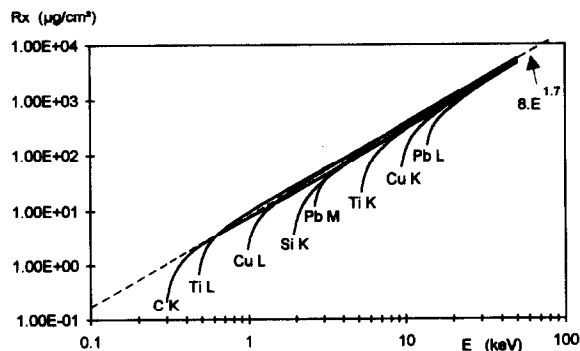


Fig. 1. Ultimate ionization depth vs. accelerating voltage in pure targets, according to the PAP model.

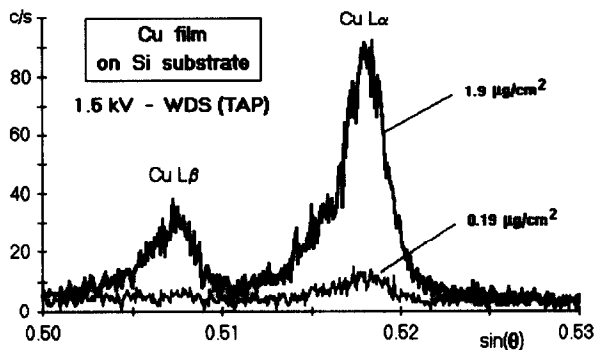


Fig. 2. WDS spectrum in the Cu L lines region corresponding to Cu layers on Si substrate. Layer thicknesses 1.9 and  $0.19 \mu\text{g}/\text{cm}^2$  ( $\sim 2$  and  $0.2 \text{ nm Cu}$ ). Accelerating voltage 1.5 kV. Beam current 150 nA. TAP monochromator. Camebax microprobe.

most favourable situation (electrons with an energy of about 1 keV generating soft x-rays). In spite of this poor resolution in depth, the technique offers however an interesting sensitivity to the surface: Fig. 2 demonstrates that a segregation of Cu less than  $0.1 \mu\text{g}/\text{cm}^2$  (equivalent to about 0.1 nm pure Cu) on top of a Si substrate can actually be detected by wavelength dispersive spectrometry (WDS). Figure 3 shows that with an energy dispersive (ED) spectrometer, although the limit of detection is slightly poorer because of a less favourable peak-to-background ratio, it still remains of the order of  $0.1 \mu\text{g}/\text{cm}^2$ . It can be noted that for the thinnest layer ( $0.19 \mu\text{g}/\text{cm}^2$ ) shown on Figs. 2 and 3, the Cu L $\alpha$   $k$ -ratio would be 3.2% at 1.5 kV and 0.67% at 2.5 kV. Even for very light elements, the sensitivity to surface seg-

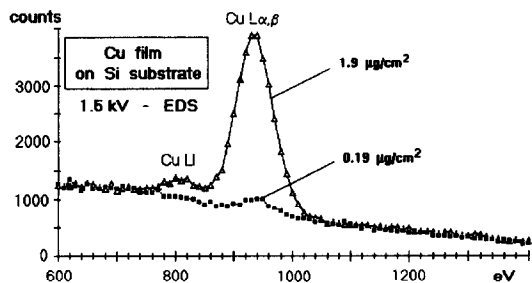


Fig. 3. ED spectrum in the Cu L lines region corresponding to the same specimen as in Fig. 2. Accelerating voltage 1.5 kV. Super Quantum Kevex Si(Li) detector. Zeiss DSM 960 scanning electron microscope.

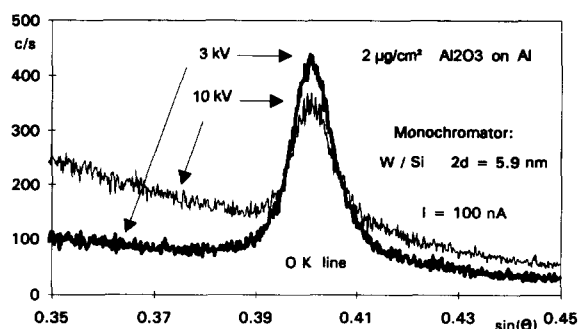


Fig. 4. WDS spectrum of the oxygen K line corresponding to a surface oxide layer on mechanically polished aluminium (mass thickness of  $\text{Al}_2\text{O}_3 \sim 2 \mu\text{g}/\text{cm}^2$ ). Accelerating voltages 3 and 10 kV. Beam current 100 nA. Multilayer W/Si monochromator. Camebax microprobe.

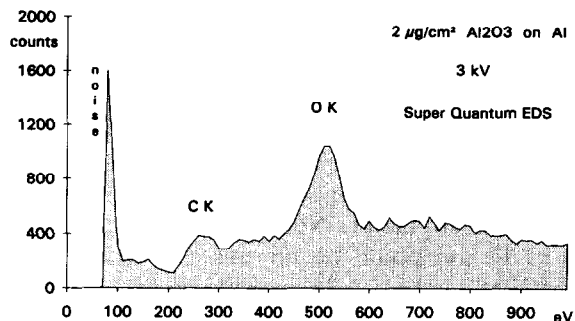


Fig. 5. ED spectrum of the same specimen as in Fig. 4. Accelerating voltage 3 kV. Kevex Super Quantum Si(Li) detector. Zeiss DSM 960 scanning electron microscope.

TABLE 1

Peak count rates and peak-to-background ratios measured for  $M\alpha$  and  $L\alpha$  lines of pure Pb at low overvoltage. (Camebax microprobe. Vertical spectrometers with PET monochromator for M line and LiF monochromator for L line. Beam current 100 nA)

Line (critical energy)	Accelerating voltage (kV)	Excited depth (nm)	Overvoltage ratio	Net count rate (counts $\text{s}^{-1}$ )	Peak to background ratio
Pb $M\alpha$ (2.5 keV)	2.7	15	1.08	10	5
	2.8	20	1.12	25	12
	3.7	50	1.48	40	50
Pb $L\alpha$ (13.05 keV)	13.8	150	1.06	140	0.5
	14.2	200	1.09	320	1.1
	15.0	300	1.15	1050	2.9

TABLE 2

Peak count rates and peak-to-background ratios measured for  $L\alpha$  and  $K\alpha$  lines of pure Cu at low overvoltage (Camebax microprobe. Inclined spectrometer with TAP monochromator for L line. Vertical spectrometer with LiF monochromator for K line. Beam current 100 nA)

Line (critical energy)	Accelerating voltage (kV)	Excited depth (nm)	Overvoltage ratio	Net count rate (counts $\text{s}^{-1}$ )	Peak to background ratio
Cu $L\alpha$ (0.933 keV)	1.26	10	1.34	150	60
	1.67	20	1.80	700	80
	2.84	50	30.4	2700	100
	3.46	70	3.71	4200	105
	4.10	100	4.40	5800	110
Cu $K\alpha$ (8.98 keV)	9.46	70	1.05	110	4
	9.70	100	1.08	350	11
	10.14	1500	1.13	1000	24
	10.60	2000	1.18	2000	40
	11.76	3000	1.31	5500	75

regation is high: Figures 4 and 5 show that an oxygen amount of  $\sim 1 \mu\text{g}/\text{cm}^2$  at the surface of a freshly polished aluminium standard (such an oxygen amount corresponds to  $\sim 5 \text{ nm}$  oxide) is strongly above the limit of detectability, since it gives at 3 kV, which is not a very low accelerating voltage, a peak-to-background ratio close to 5 with a WDS spectrometer and close to 1.7 with an ED spectrometer. Note that the  $k$ -ratios of the O K line would be for this thin oxide film about 3.5% at 3 kV, 1.3% at 5 kV, and 0.4% at 10 kV.

As a general rule, if very thin films have to be characterized, one should preferably use soft characteristic lines and operate at low accelerating voltage, to combine a low depth of excitation with a degree of excitation of the atomic shells sufficient to obtain a favourable peak-to-background ratio. Thus, for the high  $Z$  elements, the M lines should be preferred to the L lines (Table 1); similarly, the L lines of the medium  $Z$  elements would give more sensitivity to near-surface applications than the K lines (Table 2). However, some of these lines have to be used with great care; for example, the  $L\alpha$  lines of the transition elements of the 4th period (Sc to Ni) can be a source of problems in the quantitation, since they exhibit significant changes in their intensity and in their coefficients of self-absorption, depending on chemical bonding [7].

The capability of detecting elements located at some distance below the surface depends firstly on the electron accelerating voltage. The highest voltage available in the commercial instruments (scanning electron microscope or electron probe microanalyzer) is generally between 30 and 50 kV. Figure 1 shows that in such conditions, the ultimate ionization depth is of the order of a few  $\text{mg}/\text{cm}^2$  (i.e. a few micrometers for a target with a density of  $10 \text{ g}/\text{cm}^3$ ). When a buried layer is excited by the electrons, the capability of detecting an element present in this layer depends on the mass thickness of this element, but also on the absorption of its characteristic radiation, which depends on the mass thickness and on the nature of the material(s) covering the buried layer. This will be illustrated in the next paragraph.

#### DISTRIBUTION IN DEPTH OF THE PRIMARY IONIZATION

Several rough approximations of the depth distribution of ionizations, called  $\phi(\rho z)$  by Castaing [1], have been used for a long time to perform the absorption correction in the conventional ZAF procedure for quantitative analysis. The most popular have been the exponential model of Philibert [8] and the square model of Bishop [9]. The latter had the interest of demonstrating that even with an oversimplified model, satisfactory absorption corrections could be obtained in many cases, provided that the mean depth for x-ray generation was well parameterized. Unfortunately, these approximate models were not able to produce good quantitative results in the case of light element analyses (B, C, N, O...) and could not be applied successfully to stratified specimens, in spite of several attempts.

During the 1980s, new models based on more realistic descriptions of the  $\phi(\rho z)$  distribution have been developed. As far as we know, the three models below are employed in most laboratory or commercial software packages presently available.

(i) The MSG (modified surface-centered Gaussian) model of Packwood and Brown [2,3] is based on a random walk approach, which leads to describe the  $\phi(\rho z)$  function by a surface-centred gaussian, which, however, has to be modified by an exponential transient near the surface to account for the progressive scattering of the beam penetrating the specimen:  $\phi(\rho z) = \gamma \{1 - [\gamma - \phi(0)]/\gamma \exp(-\beta\rho z)\} \cdot \exp[-(\alpha\rho z)^2]$ . Four shape parameters define the distribution: the width  $1/\alpha$  of the gaussian (the calculation of which involves mainly the Bethe electron slowing down expression); the amplitude  $\gamma$  of the gaussian (which involves the ionization cross-section); the actual value  $\phi(0)$  of the distribution at the surface (which involves mainly the electron backscattering coefficient); the argument  $\beta$  of the exponential term, which alters the pure gaussian near the surface. The original parameters of Packwood and Brown have been revised by Bastin to improve the results for light element analyses. However, when it

is based on the above shape parameters, the resulting  $\phi(\rho z)$  function leads to difficulties for the evaluation of the so-called atomic number effects. It is why, instead of relating empirically the argument  $\beta$  to  $\alpha$  as in the initial approach, Bastin et al. [10] later proposed to set it so that the  $\phi(\rho z)$  distribution would have the same area as in the models of Pouchou and Pichoir.

(ii) The PAP model by Pouchou and Pichoir [4–6] uses two connected parabolas to describe the distribution:  $\phi(\rho z) = a_1(\rho z - R_m)^2 + \phi(0)$  from  $\rho z = 0$  to  $R_c$  (connection point) and  $\phi(\rho z) = a_2(\rho z - R_x)^2$  from  $\rho z = R_c$  to  $R_x$  (ultimate ionization depth). The model has been designed to be in agreement with the definition of  $\phi(\rho z)$  by Castaing, i.e. the area  $F$  of  $\phi(\rho z)$  is proportional to the number  $N_j$  of primary ionizations produced per incident electron on the level  $j$  of atoms A:  $N_j = C_A N^o Q_j(E_0) F / A$ .

$Q_j(E_0)$  is the ionization cross section of level  $j$  at initial electron energy  $E_0$ ;  $\rho$  is the specific weight of the target;  $A$  is the atomic mass of the element;  $C_A$  is its mass concentration;  $N^o$  is the Avogadro's number). The computation of  $N_j$  involves expressions for the electron energy loss  $dE/d\rho s$ , the ionization cross-section, and the losses  $1 - R$  due to backscattered electrons:

$$N_j = C_A (N^o / A) R \int_{E_0}^{E_j} Q_j(E) / (dE/d\rho s) dE$$

In addition to the fundamental area parameter, three shape parameters are used to define completely the distribution: the ultimate ionization range  $R_x$  for the level of interest, the location of the maximum of the distribution  $R_m$  and the surface ionization  $\phi(0)$ . The PAP model has been principally parameterized on the basis of stratified specimen experiments. It has been shown to give reliable results in this field as well as for light element analysis [11–14].

(iii) The XPP model is the latest model produced by Pouchou and Pichoir [6,15]. The aim was to build a reliable but simple mathematical model, able to describe properly with a single set of expressions the  $\phi(\rho z)$  distribution even at oblique electron beam incidence (this allows to use it efficiently in all practical EDS/SEM situa-

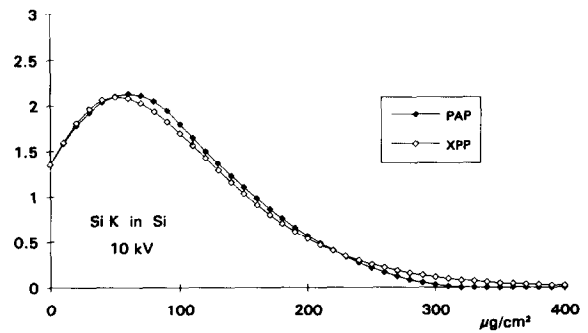


Fig. 6. Comparison of the  $\phi(\rho z)$  functions predicted by PAP and XPP models for the Si K $\alpha$  radiation in pure Si.

tions). A satisfactory description of the distribution is obtained by combining exponential and linear functions, as follows:  $\phi(\rho z) = a \exp(-\alpha \rho z) + [\phi(0) - a] \cdot \exp(-\beta \rho z)$ . The basic parameter is still the area below the  $\phi(\rho z)$  curve, as in the PAP model. The surface ionization  $\phi(0)$  is also unchanged; the two other shape parameters are the mean depth for x-ray generation  $R_b$  and the slope of the distribution at the surface  $\phi'(0)$ . A unique feature of XPP is that its parameters are expressed as a function of the specimen tilt angle [16].

Figures 6 and 7 compare the  $\phi(\rho z)$  distributions predicted by PAP and XPP models for Si K ionizations by 10 keV electrons in light and heavy targets (pure Si and the  $\text{ReSi}_2$  compound) at normal beam incidence. Although the models use different mathematical descriptions, it can be verified that they produce very similar distributions.

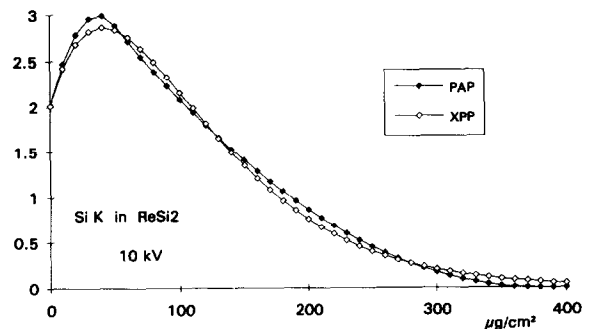


Fig. 7. Comparison of the  $\phi(\rho z)$  functions predicted by PAP and XPP models for the Si K $\alpha$  radiation in the compound  $\text{ReSi}_2$ .

It is also interesting to note that for a given line at a given voltage, the ultimate ionization depth (expressed in mass units) does not depend strongly on the atomic number of the target. This is a great advantage in the study of layered specimens, since it permits to estimate the excited depth without knowing the nature of the specimen. In practice, if an estimation of the ionization depth is needed, for example to initialize a procedure, the following modification of the Castaing formula can be used ( $R_x$  in  $\mu\text{g}/\text{cm}^2$ ,  $E_0$  and  $E_j$  in keV):

$$R_x = 8(E_0^{1.7} - E_j^{1.7})g(U_0)$$

with

$$g(U_0) = 1 + 3/[E_j^{0.5}(U_0 + 0.3)^2] \text{ and } U_0 = E_0/E_j$$

When soft x-rays are used for the analysis, one has to be aware that the actual depth of analysis for these lines may differ strongly from the excited depth, because of the influence of absorption. Figures 8 and 9, relative to the oxygen K line respectively in chromium and titanium at 5 and 15 kV, illustrate this point. Although Cr and Ti are very close in the periodic table, they behave differently for the oxygen analysis, because they have very different mass absorption coefficients for the O K line:  $\mu/\rho = 2900 \text{ cm}^2/\text{g}$  in Cr and  $22100 \text{ cm}^2/\text{g}$  in Ti. While in Cr (Fig. 8) the distribution of the emerging intensity changes significantly with the accelerating voltage (the maximum effective depth of x-ray emission drops from 100 to about  $500 \mu\text{g}/\text{cm}^2$  from 5 to 15 kV),

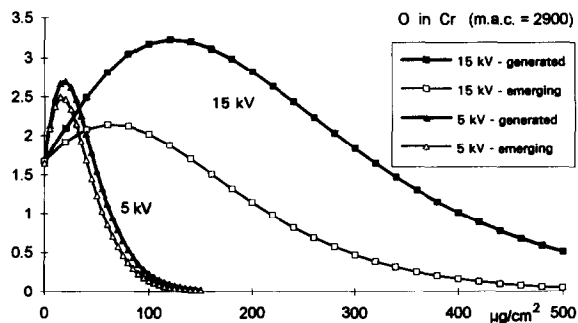


Fig. 8. Distributions of the generated and of the emerging O K $\alpha$  intensity at 5 and 15 kV in a Cr matrix (40° take-off angle assumed).

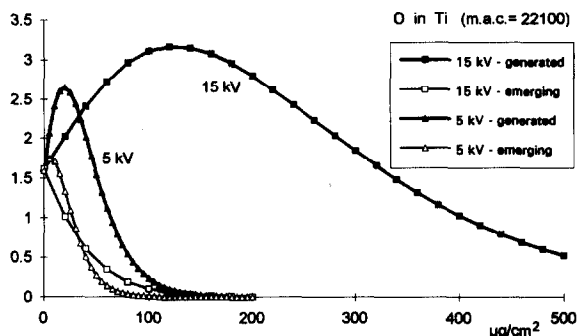


Fig. 9. Distributions of the generated and of the emerging O K $\alpha$  intensity at 5 and 15 kV in a Ti matrix (40° take-off angle assumed).

the effective depth of O K emission in a Ti matrix (Fig. 9) is almost independent of the voltage, and is limited to about  $100 \mu\text{g}/\text{cm}^2$  by the strong absorption in Ti.

#### USE OF THE $\phi(\rho z)$ FUNCTION FOR LAYERED SPECIMENS

In the general case of a stratified specimen, a layer of index  $s$  located from mass depth  $\rho z_s$  to  $\rho z_{s+1}$  and containing element A with mass concentration  $C_A^s$  emits in a characteristic line of A a x-ray intensity proportional to:

$$I_A^s = C_A^s T_A^s \int_{\rho z_s}^{\rho z_{s+1}} \phi_A(\rho z) \exp(-\chi_A^s \rho z) d\rho z$$

with

$$T_A^s = \prod_{k=1}^{s-1} \exp[\Delta\rho z_k (\chi_A^s - \chi_A^k)]$$

$T_A^s$  takes into account the absorption of A radiation emitted in layer  $s$  by the upper layers of mass thicknesses  $\Delta\rho z_k = \rho z_k - \rho z_{k-1}$ .  $\chi_A^s$  and  $\chi_A^k$  are the absorption factors of A radiation in the layers  $s$  and  $k$  ( $\chi = \mu/\rho \text{csc}\theta$ ).

The intensity of a bulk standard would be obtained by setting  $T_A^s = 1$  and by integrating from  $\rho z = 0$  to infinity (or  $R_x$  for the PAP model). The above expression is general, and is valid for every  $\phi(\rho z)$  model.

In the analytical  $\phi(\rho z)$  models presently available, it is assumed that the distribution is not basically different in a layered target and in a

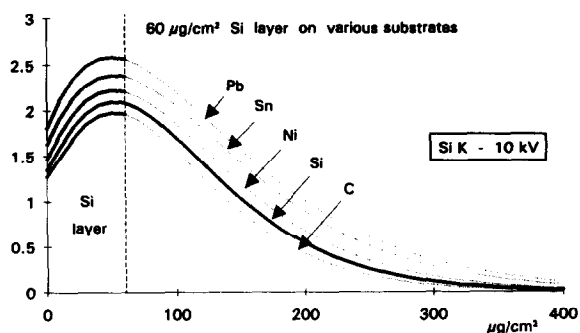


Fig. 10.  $\phi(\rho z)$  functions of a  $60 \mu\text{g}/\text{cm}^2$  Si layer ( $\sim 250 \text{ nm}$ ) for light to heavy substrates. Si  $K\alpha$  line at 10 kV. XPP model.

homogeneous target which would have the same mean atomic number. Obviously, this assumption is strictly valid only when the layers have similar diffusion and stopping powers of the impinging electrons (i.e. when the layers have similar mean atomic numbers). In most cases where these conditions are not satisfied, the basic parameters of every  $\phi(\rho z)$  model can be computed with a satisfactory accuracy by use of an appropriate weighting law for each of them [3,6,17]. Figures 10 and 11 illustrate for the XPP model the distortion of the  $\phi(\rho z)$  curve predicted by such a weighting method in the case of a Si layer on different substrates and for Si layers of variable thickness on a heavy substrate. However, it should be pointed out that when the layers have very different atomic numbers, the approximation of a progressive distortion of the  $\phi(\rho z)$  curves becomes more questionable: Monte-Carlo simulations actually indicate that non negligible distortion of

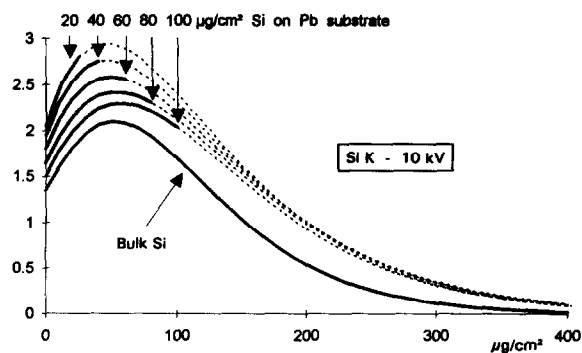


Fig. 11.  $\phi(\rho z)$  functions of Si layers of variable thickness on a heavy Pb substrate. Si  $K\alpha$  line at 10 kV. XPP model.

the  $\phi(\rho z)$  curves may appear near the interfaces [18]. In the case of a single layer on a substrate, the most critical situation occurs for extreme differences in the atomic numbers (e.g. very light element on heavy substrate), and when the depth of the interface is of the order of half the ultimate ionization depth. In these particularly unfavourable situations, we believe that the error on the computed intensities may reach up to 20% relative. Fortunately, for all the elements of a given layer, the error is almost the same. Hence, since the process of simultaneous determination of thickness and composition of a layer requires to normalize the concentrations, the error on the chemical analysis is limited, and most of the uncertainty lies in the thickness determination. In those extreme situations where the quantitation may become uncertain, the operator should always try to select the most appropriate analytical conditions. For example, in the case of a thin film of low atomic number at the surface of a heavy substrate, it may be better, even if the experimental peak-to-background ratio becomes poorer, to operate at a rather high voltage, so that the film will appear very thin compared to the ultimate ionization depth. Hence, it will become possible to approximate almost perfectly the  $\phi(\rho z)$  curve of the specimen by that of the substrate.

Before introducing the computer programs available for the characterization of layered specimens, it is useful to explain with simple arguments how a set of  $k$ -ratios makes it possible to get simultaneously the mass thickness and the composition of a layer on a substrate, and to correlate this with the conventional analysis of homogeneous volumes. Basically, in the case of homogeneous volumes, it is not necessary to analyze all  $N$  elements present in the sample: the analysis of  $N - 1$  elements and the computation of the last one by difference is actually sufficient. In practice however, all the elements are generally measured when possible, because the extra information allows to check that the sum of the concentrations is close to 100%. In the case of stratified specimens, one can use the extra information given by the sum of the  $k$ -ratios to deduce the mass thickness of the layer, provided that all the elements of the layer are measured and that

their concentrations are normalized at each step of the computation.

#### THE STRATA AND MULTIFILM PACKAGES

*Strata* and *Multifilm* are two software packages developed in cooperation with SAMx for advanced applications in x-ray microanalysis, mainly for the characterization of surface segregation and stratified specimens.

*Strata* is available either in a *PC / Windows* or in a *SUN / Sunview* version; it is a general purpose and user-friendly off-line program that uses *k*-ratios as input data. *Multifilm*, which has been specially designed for the Kevex ED spectroscopy system, can additionally handle Kevex ED spectra directly to produce a *k*-ratio file. Both programs enable to process data measured at one or several accelerating voltages. The voltage(s) can be completely different from one element to another. Either the PAP model or the XPP model can be applied. The latter allows to use oblique electron beam incidence.

The latest version of *Multifilm* offers also a ASAP option ("as soon as possible"). Whatever the number of elements to be analyzed, and whatever the number of accelerating voltages used, the ASAP mode allows to measure only a limited set of standards (at least one, which does not necessarily needs to contain an element present in the specimen). The x-ray intensities of all missing pure standards are then computed on the basis of the measured one(s). Contrary to the case of conventional analysis of homogeneous microvolumes, it is not easy in the case of stratified specimens to work with no standard at all, because this would require to know very accurately the beam current and the solid angle of detection. This is why *Multifilm*/ASAP requires at least one standard. Presently, the ASAP quantitation may be applied successfully for K lines. For L and M lines, further basic work is needed, because some physical parameters involved in the computation of the characteristic L and M intensities (namely the Coster-Kronig radiationless transition rates and the relative weights of the

lines in a series) are not known presently with enough accuracy [15,20,21].

The *Strata* and *Multifilm* programs both include the secondary emission due to the fluorescence excited by characteristic lines and by the x-ray continuum. The formulae developed by the authors are used [6]. The implementation of the fluorescence by the continuum has led to a revision in the original PAP and XPP models of the expressions for the primary intensity [19]. Taking into account both types of fluorescence is very important; actually, in some cases where high energy radiation is used, omitting the secondary emission can lead to strong errors, even when only a qualitative understanding of the experimental data is required. Since a full computation of the fluorescence at several voltages and for a layered specimen requires time (the computing time almost doubles when the fluorescence is included), a switch in the program allows skipping this secondary effect, if so desired. Actually, the fluorescence may be neglected every time only soft x-rays (with energy in the keV region or less) are considered, but it must definitely be taken into account for more energetic lines. Several experimental examples have already shown [6,16] that, although the excitation by fluorescence is for every atom of the target a low probability event compared to the primary ionization by electrons, the secondary emission represents, as a whole, a non negligible intensity since it is produced in a volume larger by several orders of magnitude than the primary emission (the range of excitation by 10 keV photons is typically 10 times the range of excitation by 20 keV electrons). Figure 12 gives a set of theoretical curves computed with the *Strata* program, showing the contribution of the fluorescence in the simple case of Zn coatings (0.2 to 5  $\mu\text{m}$  thickness) on a Cu substrate. At the lowest voltages, just above the Zn K critical energy, one can observe that, because of the fluorescence by the continuum, the *k*-ratio for the Zn  $K\alpha$  line is not equal to 1, but lies between 0.93 and 1 (the amount of Zn that can be excited by fluorescence is less in the film than in a bulk standard). On the other hand, at voltages just above the Cu K critical energy where the electrons are not able to produce Cu K exci-

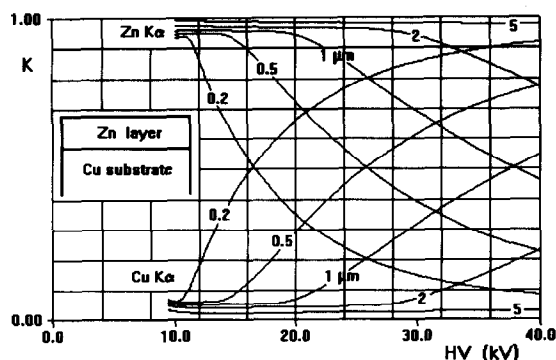


Fig. 12. Curves of Zn  $K\alpha$  and Cu  $K\alpha$   $k$ -ratios vs. accelerating voltage for Zn layers of different thicknesses (0.2 to 5  $\mu\text{m}$ ) on a Cu substrate, showing the fluorescence mainly due to the excitation by the continuum ( $40^\circ$  take-off assumed).

tations in the substrate, the Cu  $K\alpha$   $k$ -ratio is not zero, but lies between 0 and 7%, depending on the layer thickness. In the present case, this represents mainly the excitation of the substrate by the continuum, since the excitation of Cu by the Zn  $K\beta$  line is only a small fraction of the total fluorescence effect. It should be pointed out that for the thickest Zn film (5  $\mu\text{m}$ ), no primary ionization of the Cu substrate occurs up to 40 kV, but the Cu fluorescence emission still represents about 3% of the intensity of a pure bulk Cu standard. This shows the danger of assuming that a thick film is equivalent to a bulk specimen and of analyzing it by means of conventional software programs, which neglect most often the fluorescence by the continuum. We believe that this is a frequent source of misinterpretation of x-ray microanalysis data.

#### OPERATING STRATA AND MULTIFILM PROGRAMS

*Strata* and *Multifilm* offer two principal modes of operation, and additional accessory features.

(1) The more general mode is a graphical mode called "K vs. HV", in which  $k$ -ratios curves are calculated and displayed as a function of the accelerating voltage, for a given description of the specimen (mass thicknesses and compositions of the layers). In this mode, the specimen description may be either a hypothesis of the operator

(as in Fig. 12), or the result of another working mode, the iterative mode. It is very useful to operate "K vs. HV" prior to an experiment, to verify if one can reasonably expect to solve a given problem, and to define the best operating conditions for this problem (analytical line, voltage range ...). "K vs. HV" can also be used after the experiment, to process the data by a trial and error approach, in which the operator formulates reasonable hypotheses, to obtain the best agreement between the calculated and the experimental  $k$ -ratios. This operating mode is of general use and can be applied in any case. However, this does not imply that all problems can be solved completely with this method: it should not be forgotten that, in complex cases, a satisfactory agreement between computed and experimental  $k$ -ratios can be obtained for several hypotheses on the specimen structure! Starting from the 3.0 version, *Strata* provides a forward and backward switch, from the "K vs. HV" display to a "K vs.  $R_x$ " display, which may help in understanding the structure of the specimen (for a given line,  $R_x$  is the ionization depth corresponding to HV). On a "K vs.  $R_x$ " graph, the elements located in the same layer appear at the same abscissa, whatever their critical energy, unlike on a "K vs. HV" plot.

(2) The other important operating mode is the automatic mode, whereby the thicknesses and the compositions of the strates can be obtained simultaneously by an iterative procedure. This powerful mode of operation can be applied under certain conditions:

(i) all elements in a layer of unknown composition should be measured, except those determined by stoichiometry;

(ii) all the layers to be chemically characterized (including the substrate) should be excited, and their radiation should not be completely absorbed by the upper layers;

(iii) an element may be present in several layers, but it is allowed to have an unknown concentration in one layer only. (It is recalled that an element determined by stoichiometry is not considered as having an unknown concentration);

(iv) every layer is supposed to have a uniform composition.

In order to determine concentrations and thicknesses, different iterative schemes are used, depending on whether some elements (index  $i$ ) are present in several layers (index  $s$ ) or not. In both cases, at each iteration step  $j$ , the concentrations  $C_j(i, s)$  and the thicknesses  $T_j(s)$  are determined inside separate loops. The concentrations are always obtained by a simple iteration:  $C_{j+1}(i, s) = C_j(i, s)$ .  $K_{\text{exp}}(i)/K_{\text{calc}}(i)$ . Here,  $K_{\text{exp}}(i)$  represents the experimental  $k$ -ratio of element  $i$  at a given voltage, and  $K_{\text{calc}}(i)$  the computed value corresponding to the current specimen description.

When there is no common element, the thicknesses are also determined by simple iteration:

$$T_{j+1}(s) = T_j(s) \sum_i K_{\text{exp}}(i) / \sum_i K_{\text{calc}}(i).$$

When there are common elements, we adopted a different iteration scheme. The concentrations are still computed by a simple iteration, as in the previous case. But for the thicknesses, the iterative technique is to look for the least deviation  $\Delta$  between the calculated  $k$ -ratios  $K_{\text{calc}}(i)$  and the experimental data  $K_{\text{exp}}(i)$ . The thickness leading to the least deviation is estimated from the deviations  $\Delta^0$ ,  $\Delta^+$  and  $\Delta^-$  corresponding respectively to the current thickness  $T_j$ , to  $T_j + \delta T_j$  and to  $T_j - \delta T_j$  (a convenient value for  $\delta T_j$  is  $T_j/20$ ). The iteration is stopped when all the concentrations and thicknesses are stationary within  $10^{-4}$ .

(3) Two accessory working modes of the *Strata* and *Multifilm* programs are the plot of  $\phi(\rho z)$

curves (see Figs. 6–11). Starting from the 3.0 version, *Strata* also enables to compute and plot calibration curves of  $k$ -ratios versus the mass thickness, for layers of known composition on a known substrate.

#### EXAMPLES OF STRATA OR MULTIFILM APPLICATION

The examples in this paragraph illustrate different types of applications of *Strata* or *Multifilm*, from very simple situations to more complex ones. In the following examples, the thicknesses will frequently be expressed in Angströms, nanometers or micrometers for an easier understanding. However, it should be emphasized that only mass thicknesses make sense and can actually be determined by the technique. The use of linear thicknesses implies that a value of the density is assumed in the computation. If not specified, the nominal density of the bulk material is assumed.

##### Example 1: bilayer on substrate (no common element)

The first example is a typical problem of simultaneous determination of thickness and composition for which no other method can give a reliable result as easily and as quickly as XRMA can do. An experiment of Willich [14] has been selected. The specimen consists of two layers (Ni–Cr

Layer #	Element	# atoms	Mass thck. (µg/cm <sup>2</sup> )	Thck. (Å)	Density
1	Ni	0.0000	7.4	100.0	7.41
	Cr	0.0000			
2	Fe	0.0000	10.6	100.0	10.60
	Gd	0.0000			
	Pt	0.0000			
Substrate	Si	1.0000			

Fig. 13. Specimen description window of the *Strata* software before applying the iteration to the experimental  $k$ -ratios of Table 3.

TABLE 3

$k$ -ratios for Ni, Cr and Fe  $K\alpha$ , Gd  $L\alpha$  and Pt  $M\alpha$  (from [14]) used by *Strata* for the characterization of the layered specimen described in Figure 13 (take-off  $40^\circ$ )

$E_o$ (keV)	Ni $K\alpha$	Cr $K\alpha$	Fe $K\alpha$	Gd $L\alpha$	Pt $M\alpha$
20	0.0151	0.0744	0.0258	0.0123	0.0083
25	0.0084	0.0443	0.0147	0.0076	0.0058
30	0.0054	0.0299	0.0098	0.0052	0.0048

and Fe–Gd–Pt) on top of a Si substrate. The  $k$ -ratios of the Ni, Cr and Fe  $K\alpha$  lines, of the Gd  $L\alpha$  line and of the Pt  $M\alpha$  line, measured with respect to pure standards at 20, 25 and 30 kV are given in Table 3. Figure 13 is the initial description of the problem in *Strata* (the unknown concentrations are set to zero, the unknown thicknesses of both layers are initialized to 100 Angströms, the assumed densities are respec-

tively 7.41 and 10.60). Figure 14 shows a black and white copy of the screen at the end of the iteration, using the PAP model with full fluorescence effects (lines and continuum). After 5 iterations, the compositions and mass thicknesses of both layers are obtained, with a mean relative deviation between the experimental data and the computed  $k$ -ratios slightly less than 1%. For this specimen, the technique of Rutherford Backscattering Spectrometry is applicable, and can give the same type of information. Table 4 shows the excellent agreement between the results of *Strata* and the RBS results reported by Willich. After the iterative process, the “K vs. HV” mode of *Strata* can be executed to check the agreement between the computed curves and the experimental data (Fig. 15). This comparison may also be done by switching to the “K vs.  $R_x$ ” mode (Fig. 16). The interest of the latter mode is obvious: as

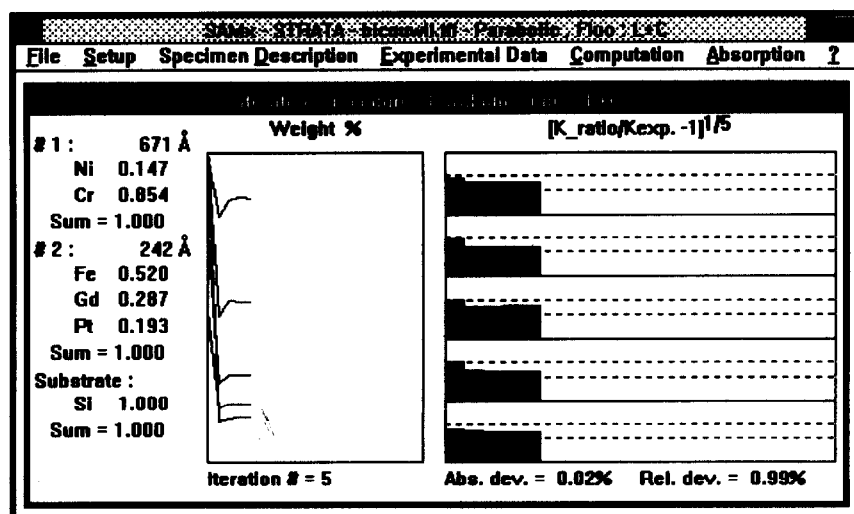


Fig. 14. Iteration window of the *Strata* software at the end of the iterative procedure.

TABLE 4

Comparison of the XRMA results using *Strata* with the RBS results for a Ni–Cr/Fe–Gd–Pt/Si stratified specimen (experimental data from [14])

	Surface layer			Buried layer			
	wt.% Ni	wt.% Cr	Thickness (nm)	wt.% Fe	wt.% Gd	wt.% Pt	Thickness (nm)
XRMA	14.7	85.4	67.1	52.0	28.7	19.3	24.2
RBS	14.4	85.6	68.3	51.4	28.6	20.0	24.6

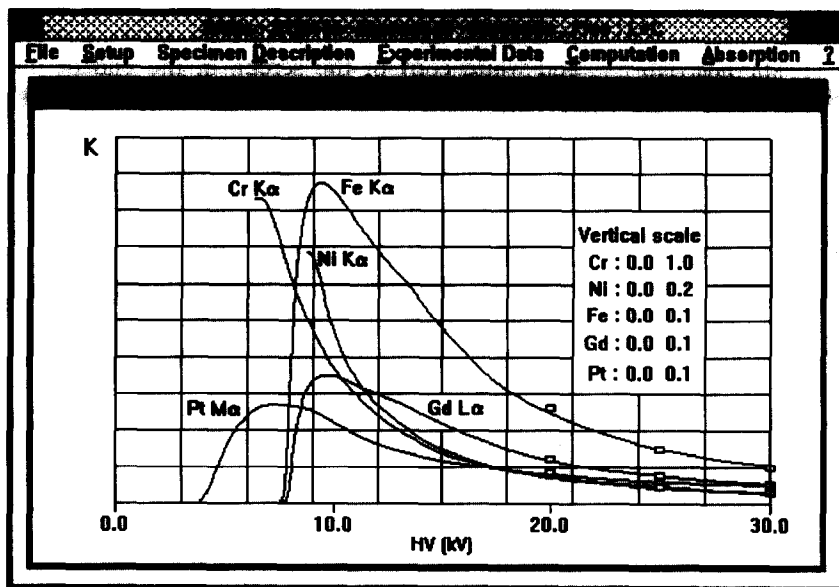


Fig. 15. Comparison of the experimental  $k$ -ratios of Table 3 with the "K vs. HV" curves computed as a function of accelerating voltage for the specimen description of Fig. 14.

mentioned earlier, the curve corresponding to the Pt  $M\alpha$  line lies in the same  $R_x$  range as the curves for Fe and Gd (elements present in the same layer), whereas in the "K vs. HV" display mode, the curve for Pt  $M\alpha$  was appearing at a

lower energy, because of its critical excitation energy significantly lower than the Fe K and Gd  $L_3$  levels. This example gives the opportunity of four additional comments:

(i) since there is no common element in the

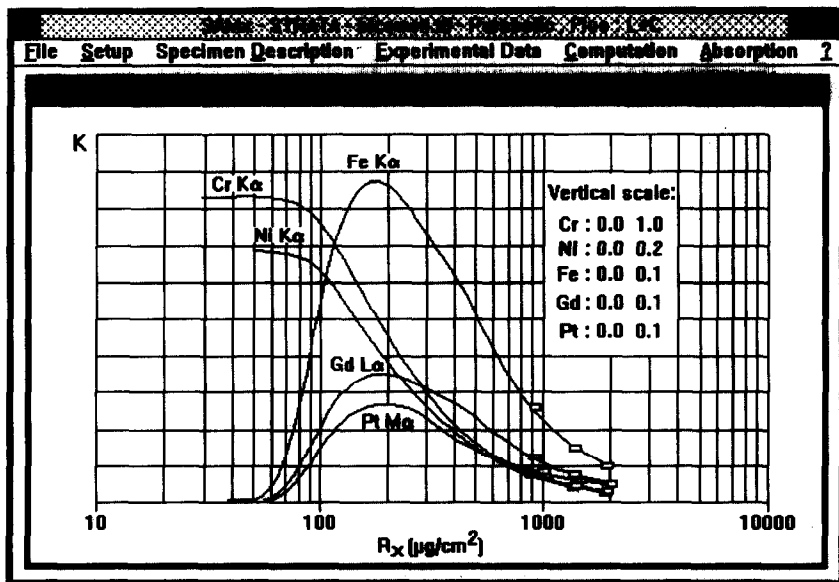


Fig. 16. Comparison of the experimental  $k$ -ratios of Table 3 with the "K vs.  $R_x$ " curves plotted vs. the ultimate excitation depth for the specimen description of Fig. 14.

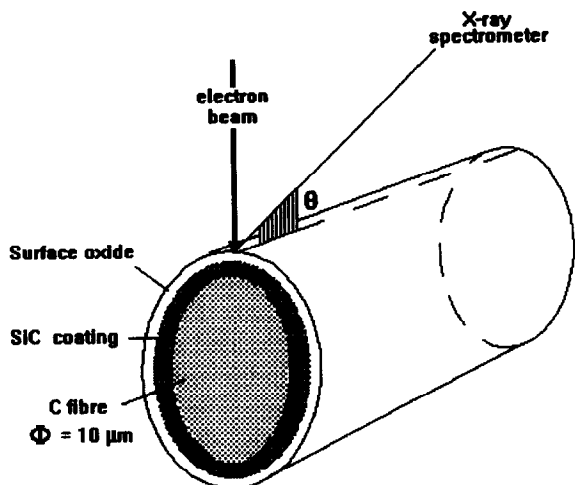


Fig. 17. Analytical geometry used for in-depth analysis of a coated fibre.

different strates, the sum of the concentrations obtained for both strates is necessarily 100%;

(ii) since there is no common element in the different strates, it would have been sufficient to measure the *k*-ratios at a single voltage to get the full information. The measurements at three different voltages were made just to verify the consistency of the results;

(iii) it can be observed that the measurements have been made at rather high voltages. In such conditions, the films represent a small fraction of the excitation range, so that the *k*-ratios are small and the peak-to-background ratios are poor. Consequently, a great care is needed in the measurements to avoid systematic errors and ensure a sufficient statistical precision. Willich was em-

ploying such extreme conditions to be able to process the data with his own simplified software, in which it is assumed that the  $\phi(\rho z)$  function in the whole specimen can be approximated by that of the substrate. With the more sophisticated model used in *Strata*, this approximation is not needed; thus, it would be easier (mainly if an ED spectrometer was used) to perform the analysis at a lower voltage, for instance 15 kV;

(iv) in such a specimen, it would be interesting, mainly in the case of a single voltage, to measure also the *k*-ratio of the Si substrate. This additional information would allow to check the global consistency of the experiment.

*Example 2: characterization of a coating on a fibre (common elements, very light elements)*

This second example has several particularities: the geometry of the specimen, the analysis of very light elements, and the presence of common elements in several layers. The specimen is a carbon fibre (typical diameter 10  $\mu\text{m}$ ) coated with silicon carbide (thickness in the range 100-200 nm). The objective of the experiment was to control the composition of the coating and its thickness, as well as the oxidation of the coating at the surface. Because of the special shape of the specimen, and because light elements have to be analyzed, this type of experiment requires a great deal of care, mainly to avoid experimental errors that could come from a bad geometrical configuration of the specimen with respect to the spectrometer. In particular, it is essential for the electron beam to be accurately focused on top of

FILE: STRATA - Parametric Plot - Base

File Setup Specimen Description Experimental Data Computation Absorption

Valid Cancel Help Layer + - Element + -

Layer #	Element	# atoms	Mass thick. [ $\mu\text{g}/\text{cm}^2$ ]	Thick. ( $\text{\AA}$ )	Density
1	Si	1.000	2.3	100.0	2.33
	O	2.000			
2	Si	0	3.2	100.0	3.15
	C	0			
Substrate	C	1.000			

Fig. 18. Specimen description window of the *Strata* software before applying the iteration to the experimental data of Table 5.

TABLE 5

Relative intensities of C, O and Si  $K\alpha$  lines measured at several electron energies on the specimen of Fig. 17 (take-off angle  $40^\circ$ )

$E_o$ (keV)	Si $K\alpha$ (pure standard)	$E_o$ (keV)	O $K\alpha$ ( $Y_3Fe_5O_{12}$ standard)	C K (SiC standard)
2.3	0.623	1.1	0.3000	0.800
3.0	0.646	2.3	0.0780	0.900
3.5	0.646	3.0	0.0682	1.036
5	0.591	5.0	0.0240	1.149
7.5	0.346	7.5	0.0200	2.038

the fibre, and for the fibre to be oriented towards the spectrometer port (Fig. 17), so that the angle of incidence of the electrons and the take-off angle of the x-rays are well defined.

Table 5 gives the relative intensities measured for the  $K\alpha$  lines of Si, O and C in the low accelerating voltage range (1.1-7.5 kV). For oxygen analysis, a conductive  $Y_3Fe_5O_{12}$  standard was used; a SiC compound standard was used for carbon. For this element, area measurements of the emission band were necessary, as shown later.

Figure 18 is the specimen description window of *Strata* prior to the actual calculation. The

Si-C layer of unknown composition (concentrations set to zero) and of unknown thickness (initial thickness set to 10 nm) is supposed to be covered at the surface by an oxide film of composition  $SiO_2$  and unknown thickness.

This example, where two elements (Si and C) are simultaneously present in two components of the layered structure, can be solved by the iterative method, since the concentrations of Si and C are unknown in one layer only. Figure 19 shows the copy of the screen at the end of the calculation, applying the XPP model with full fluorescence effects. The procedure converges after 18 iterations, with a mean relative deviation of 2.7% between the computed and the experimental data. The Si-C layer is found to have a thickness of approximately  $53 \mu g/cm^2$  (168 nm assuming a density of  $3.15 g/cm^3$ ) and a composition very close to the SiC stoichiometry (the bottom window displays weight fractions without normalization, while the top window gives the corresponding normalized atom fractions). The thickness of the oxide film at the outer surface of the coating is found to be  $0.9 \mu g/cm^2$  (3.7 nm assuming a density of  $2.33 g/cm^3$ ).

Switching to the "K vs. HV" mode allows to compare the curves of relative intensities corre-

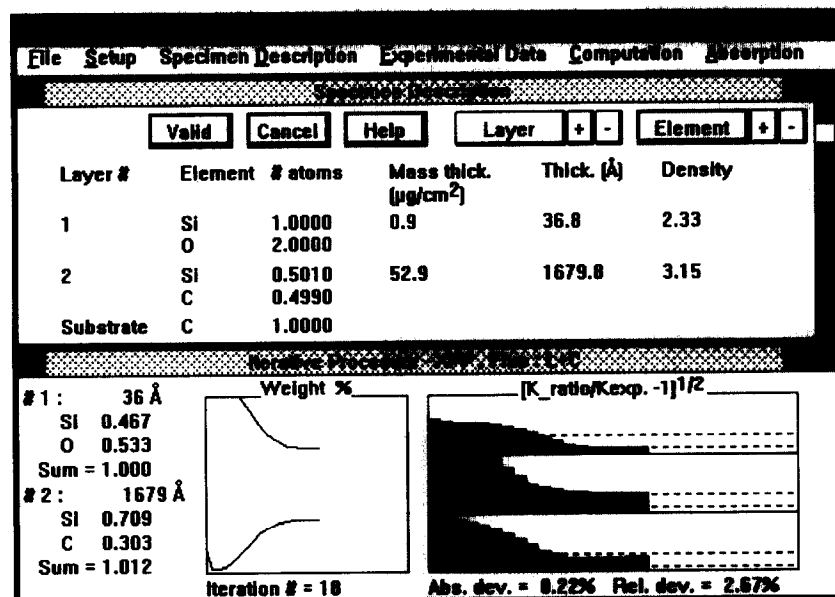


Fig. 19. Result of the *Strata* iterative procedure applied to the problem defined by Fig. 18 and Table 5.

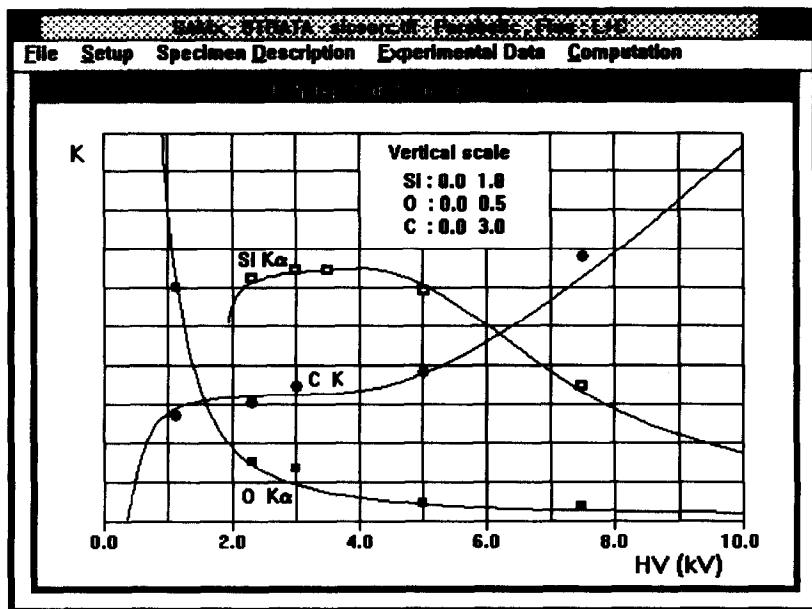


Fig. 20. Comparison of the experimental data of Table 5 with the “K vs. HV” curves computed as a function of accelerating voltage for the specimen description of Fig. 19.

sponding to this result with the experimental data (Fig. 20). It can be seen that with two accelerating voltages only (typically 3 kV and 7.5 kV), a full characterization of this particular specimen would have been possible.

Figure 21 compares the WDS spectra obtained for the C K line in different operating conditions. At 3.5 kV, the primary electrons are able to excite the SiC coating only, as can be verified on

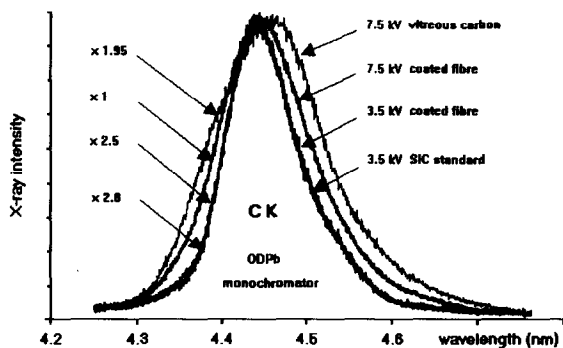


Fig. 21. WDS spectra of the C K line recorded on the SiC-coated carbon fibre at two different voltages (3.5 and 7.5 kV). Comparison with the characteristic lines of vitreous carbon and of SiC. Synthetic multilayer monochromator (W/Si 2d = 5.9 nm).

Fig. 20. Consequently, the C K band is narrow, and has the same shape as a SiC standard. On the contrary, at 7.5 kV, the electrons excite also the carbon substrate, which produces approximately one half of the emerging intensity. Hence, the C K emission band becomes wider, and tends to that of vitreous carbon (which is similar to that of an uncoated fibre). This illustrates that whenever very light elements are present in stratified specimens under different chemical forms, it is necessary to perform area measurements at every voltage, to take into account the continuous change of the line shape with the analyzed depth.

*Example 3: “As soon as possible (ASAP)” analysis of a coated substrate and determination of the coating thickness*

This last example illustrates the capability of the *Multifilm* software to characterize stratified specimens by ED spectrometry with a reduced set of standards (ASAP option). This example has two other particularities: firstly, the specimen component which is supposed to have an unknown composition is the substrate; secondly, to illustrate the wide capability of the procedure,

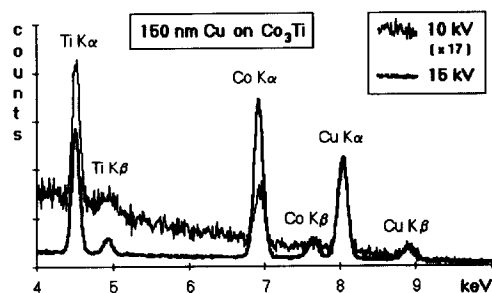


Fig. 22. ED spectra in the region of the Ti K to Cu K lines for a Cu/Co<sub>3</sub>Ti layered specimen at 10 and 15 kV. Spectra recorded at the same beam current. Normal incidence. 35° take-off angle. Super Quantum detector.

some of the measurements have been done at oblique electron beam incidence and variable take-off angle.

The specimen is a compound close to the Co<sub>3</sub>Ti composition (20.7 wt.% Ti nominal), covered by a copper layer having a thickness in the range 100–200 nm. The problem is to analyze the coated compound and to evaluate simultaneously the layer thickness. Figure 22 shows typical EDS spectra recorded at 10 and 15 kV using the same beam current and normalized at the Cu K $\alpha$  peak.

In this example, there is no common elements in the layers. Hence, one voltage is sufficient to characterize the specimen. Several spectra have

been acquired at the same voltage setting (15 kV), but in different geometrical configurations (normal or oblique incidence, variable take-off angle). In every configuration, the spectra of pure Cu, Co, Ti and additionally Cr standards have been recorded with the same beam current as the specimen spectra. Table 6 shows that the normal *Multifilm* quantitation procedure referring to the Cu, Co and Ti standards gives a composition very close to the nominal one and a Cu thickness of 144 nm in average (the assumed density is 8.96 g/cm<sup>3</sup>). In the ASAP mode, any standard can be used, even if it does not correspond to an element present in the specimen. Using only a pure Cr standard, the composition of the coated specimen and the thickness of the copper layer are found to agree very well with the results obtained using the full set of standards.

This example shows that for routine control applications, the ASAP procedure allows the user to avoid spending too much time in acquiring and processing the spectra of the standards. In the present state, we consider that its full reliability is limited to the K lines of light to medium Z elements. For the very light elements and the L and M lines, some improvements are expected as the result of the effort recently undertaken in a few laboratories to improve the standardless quantitative techniques in general [15,20–22].

TABLE 6

Characterization of a Co–Ti compound (20.7 wt.% Ti nominal) coated with pure Cu, applying the *Multifilm* program to EDS spectra acquired at 15 kV for different tilt and take-off angle [Comparison of the results obtained either using the full set of standards (Cu, Co, Ti) or using a single reference standard (“ASAP” procedure). Kevex Super Quantum Si(Li) detector. Zeiss DSM 960 scanning electron microscope]

Azimuth (deg.)	Tilt (deg)	Take-off (deg)	Full set of standards (Cu, Co, Ti)			ASAP with single Cr standard		
			Cu thickness (nm)	wt.% Co (nm)	wt.% Ti	Cu thickness	wt.% Co	wt.% Ti
0	0	35.0	141	79.1	20.9	–	–	–
0	20	55.0	150	79.5	20.5	163	79.5	20.5
40	20	48.9	142	79.7	20.3	149	79.8	20.2
60	20	42.7	140	80.0	20.0	150	80.0	20.0
80	20	36.0	144	79.6	20.4	149	79.9	20.1
100	20	29.3	147	79.3	20.7	150	79.5	20.4
Average			144	79.5	20.5	152	79.8	20.2
Relative r.m.s.			2.6%	0.4%	1.5%	4.1%	0.3%	0.3%
Deviation from nominal				+0.3%	–1.0%		+0.6%	–2.4%

### Conclusions

The potential of x-ray microanalysis under electron beam excitation is much higher than commonly considered. In particular, the technique can be applied very successfully to the detection of near-surface segregation and the characterization of stratified specimens, from 0.1 to about 1000  $\mu\text{g}/\text{cm}^2$ . The advantages of the technique are that it is local and in principle non-destructive, that it can be performed using any commercial instrument (electron microprobe or analytical scanning electron microscope), and that it provides truly quantitative compositions and/or mass thicknesses of stratified specimens. As far as the thickness range, the sensitivity and the accuracy are concerned, the capability of the method is similar to that of RBS. Hence, advanced x-ray microanalysis techniques actually fill the domain between the "surface" techniques (x-ray photoelectron and Auger electron spectrometry) and the "bulk" techniques such as x-ray fluorescence spectrometry.

The easiest problems of in-depth analysis correspond to specimens with a known layer sequence and where every element is present in a single layer. In such situations, one obtains very rapidly, by applying an iterative procedure to the  $k$ -ratios measured at a single voltage (as in conventional microanalysis), a non ambiguous chemical and in-depth characterization of the specimen. If some elements are common to several strates, but have an unknown concentration in only one of them, an other iteration scheme, which frequently requires  $k$ -ratios measured at several voltages, can be applied successfully. Any more complex specimen structure may be solved (sometimes only partially) by a graphically assisted trial and error method.

The commercial software packages *Strata* and *Multifilm* developed with SAMx are powerful tools for these applications. Since they allow to simulate many situations, they also represent a didactic means of education in the field of advanced quantitative x-ray microanalysis.

*Strata* and *Multifilm* have been developed in cooperation with SAMx under contract ON-

ERA/SAMx No. 6361. The author acknowledges J.F. Thiot and his collaborators at SAMx for their efficient contribution to the software development. The experimental contribution of D. Boivin and Y. Pioche (ONERA) is also acknowledged. *Strata* is distributed by SAMx (Support for Applications in x-ray Microanalysis), Guyancourt, France. *Multifilm* is distributed by Kevex.

### REFERENCES

- 1 R. Castaing, Thesis, University of Paris, 1951.
- 2 R.H. Packwood and J.D. Brown, *X-Ray Spectrom.*, 10 (1981) 138.
- 3 R.H. Packwood, G. Rémond and J.D. Brown, *Proc. ICXOM 11*, Univ. W. Ontario, 1987, p. 274.
- 4 J.L. Pouchou and F. Pichoir, *Proc. ICXOM 10*, *J. Physique*, 45 (1984) C2–47.
- 5 J.L. Pouchou and F. Pichoir, *Proc. ICXOM 11*, Univ. W. Ontario, 1987, p. 249.
- 6 J.L. Pouchou and F. Pichoir, *Electron Probe Quantitation*, Plenum Press, New York, 1991, p. 31.
- 7 J.L. Pouchou and F. Pichoir, *Microbeam Analysis*, San Francisco Press, 1988, p. 319.
- 8 J. Philibert, *Métaux*, 465 (1964) 157.
- 9 H.E. Bishop, *J. Phys. D: Appl. Phys.*, 7 (1974) 2009.
- 10 G. Bastin and H. Heijligers, *Electron Probe Quantitation*, Plenum Press, New York, 1991, p. 145.
- 11 P. Willich, *Proc. ICXOM 11*, Univ. W. Ontario, 1987, p. 238.
- 12 P. Willich, D. Obertop and J. Krumme, *Microbeam Analysis*, San Francisco Press, 1988, p. 307.
- 13 P. Willich and D. Obertop, *Surf. Interface Anal.*, 13 (1988) 20.
- 14 P. Willich, *Mikrochim. Acta*, Suppl., 12 (1992) 1.
- 15 J.L. Pouchou, F. Pichoir and D. Boivin, *Microbeam Analysis*, San Francisco Press, 1990, p. 120.
- 16 J.L. Pouchou, F. Pichoir and D. Boivin, *Proc. ICXOM 12* (Krakow 1989), Academy of Mining and Metallurgy Univ. Krakow, 1, 1989, p. 52; also in ONERA Report TP 157, Publ. ONERA (1989).
- 17 J.L. Pouchou and F. Pichoir, *Scanning*, 12 (1990) 212.
- 18 P. Karduck, N. Ammann and W. Rehbach, *Microbeam Analysis*, San Francisco Press, 1990, p. 21.
- 19 J.L. Pouchou and F. Pichoir, *Scanning Microscopy*, in press.
- 20 J.L. Labar, *Microbeam Analysis*, San Francisco Press, 1988, p. 253.
- 21 J.L. Labar, C.E. Fiori and R.L. Myklebust, *Proc. EMSA/MAS meeting*, San Francisco Press, 1992, p. 1636.
- 22 J.L. Pouchou and F. Pichoir, in Rios et al. (Ed.), *Electron Microscopy 92*, Univ. Granada Spain, Vol. 1, 1992, p. 293.